Available online at www.sciencedirect.com

ScienceDirect

Ceramics International 40 (2014) 2685–2690

CERAMICS INTERNATIONAL

www.elsevier.com/locate/ceramint

Synthesis of $FePO_4 \cdot xH_2O$ for fabricating submicrometer structured $LiFePO_4$/C by a co-precipitation method

Yongming Zhu, Shenzhi Tang, Haihao Shi, Huili Hu*

Department of Applied Chemistry, Harbin Institute of Technology at Weihai, Weihai 264200, China

Received 5 September 2013; received in revised form 23 September 2013; accepted 13 October 2013
Available online 22 October 2013

Abstract

Amorphous hydrated iron (III) phosphate has been synthesized by a coordinate precipitation method from equimolecular $Fe(NO_3)_3$ and $(NH_4)_2HPO_4$ solutions at an elevated temperature. Hydrated iron (III) phosphate samples and the corresponding $LiFePO_4$/C products were characterized by XRD and SEM. The electrochemical behavior was studied by cyclic voltammetry (CV) and electrochemical impedance spectroscopy (EIS). The $LiFePO_4$/C fabricated from as-synthesized $FePO_4$ delivered discharge capacities of 162.5, 147.3, 133.0, 114.7, 97.2, 91.3 and 88.5 mAh g^{-1} at rates of 0.1*C*, 0.2*C*, 0.5*C*, 1*C*, 2*C*, 3*C* and 4*C* with satisfactory capacity retention, respectively.

Keywords: $FePO_4$; $LiFePO_4$; Coordinate precipitation; Lithium ion battery

1. Introduction

The continuous increasing demand for cheaper and nontoxic rechargeable lithium ion batteries has forced researchers to find new active materials with higher performance [1]. Among these materials, Fe-based materials, which are benefited from their rare-metal-free property, have attracted extensive interest due to the low cost and environmental benignity [2,3]. In Fe-based materials, olivine-type $LiFePO_4$ has a relatively large theoretical specific capacity of 170 mAh g^{-1} based on a two-phase reaction with discharge plateau voltage of around 3.45 V versus Li/Li^+ [4]. However, the practical specific capacity of it is quite low due to the poor kinetics of lithium intercalation/deintercalation processes [5]. And, the electronic conductivity can be effectively improved by carbon coating and supervalent cation doping for $LiFePO_4$ [6]. As a matter of fact, $FePO_4$ is usually utilized as the raw material to fabricate $LiFePO_4$ to get excellent electrochemical performance [3,7–10]. By comparison with Fe^{2+} salt, Fe^{3+} salt as the raw material is low-cost and free from oxidation. In addition, some bivalent iron starting materials, such as $FeC_2O_4 \cdot 2H_2O$ and $Fe(CH_3COO)_2$, are not only expensive but also toxic [11].

Up to now, the synthesis of $FePO_4$ with narrow size distribution, abundant porous structure and large specific surface area, which will benefit the next synthetic step of $LiFePO_4$, has become hot area [12]. Several methods have been reported to synthesis $FePO_4$ particles, such as surfactant templating [12–14], fluoride route [15], biological template [16,17], homogeneous precipitation [18], hydrothermal method [19] and co-precipitation. Among these synthesis methods, surfactant templating, fluoride route and biologic template can get nanoplates, mesostructure or hollow microsphere. While expanding surface area and reducing particles scale is useful to shorten the lithium-ion transport distances and enhance ionic diffusion rate, these three methods have a problem to remove addition agent completely. Hydrothermal method, which is limited by container size, is unfit for industrialization production. Final, compare with homogeneous precipitation method, the co-precipitation method is much more easy and feasible, with only involving aqueous solutions.

In this paper, we reported the synthesis of amorphous iron phosphate particles through a facile co-precipitation route with details. Compared to the traditional co-precipitation method, the way presented here gave a low energy needed method to synthesis of $FePO_4$ with narrow size distribution, abundant porous structure and large specific surface area which was suitable for large scale projects. Amorphous hydrated iron (III) phosphate was synthesized by a

*Correspondence to: Wenhua West Road 2#, Weihai City 264209, Shandong Province, China. Tel./fax: +86 631 5687232.
E-mail address: whhhl@126.com (H. Hu).

0272-8842/$ - see front matter © 2013 Elsevier Ltd and Techna Group S.r.l. All rights reserved.
http://dx.doi.org/10.1016/j.ceramint.2013.10.055

coordinate precipitation method from equimolecular Fe$(NO_3)_3$ and $(NH_4)_2HPO_4$ solutions with using $NH_3 \cdot H_2O$ to adjust pH value at a elevated temperature. Then, the as-synthesized $FePO_4 \cdot xH_2O$ and anhydrous $FePO_4$ which has been sintered at 600 °C were used as precursor to fabricate $LiFePO_4$/C composites. As-synthesized $FePO_4 \cdot xH_2O$, anhydrous $FePO_4$ after sintered at 720 °C, and $LiFePO_4$/C were characterized by XRD and SEM. The electrochemical behavior was studied by cyclic voltammetry, electrochemical impedance spectroscopy and electrochemical capacity measurement. The $LiFePO_4$/C fabricated from as-synthesized $FePO_4$ delivered discharge capacities of 163, 147, 133, 115, 97, 91, and 89 mAh g^{-1} at rates of 0.1*C*, 0.2*C*, 0.5*C*, 1*C*, 2*C*, 3*C* and 4*C* with satisfactory capacity retention.

2. Experiment

2.1. Synthesis of precursors

$Fe(NO_3)_3$ (0.1 mol L^{-1}) and $(NH_4)_2HPO_4$ (0.1 mol L^{-1}) solutions in a stoichiometric ratio were added together slowly and then stirred for 1 h. The concentrated $NH_3 \cdot H_2O$ solution was added into the solution dropwise to adjust the pH value in the range of 2–5. And the temperature was kept at 60 °C to suppress the formation of $Fe(OH)_3$. Immediately, pale yellow precipitate was formed. The precipitates were kept in contact with the mother liquor for 30 min with stirring. Then the sample was collected by filtration, washed several times with deionized water, and dried at 100 °C under vacuum for 4 h (Fig. 1). For comparison, the concentration of $Fe(NO_3)_3$ and $(NH_4)_2HPO_4$ solutions was changed from 0.1 mol/L to 1 mol/L, and the steps were repeated.

Since the structural transformation from amorphous to α-quartz $FePO_4$ occurred at about 610–700 °C [12,14], part of the product was heated to 720 °C with a ramping rate of 10 °C min^{-1} and then was calcined at 720 °C in air for 2 h to get crystalline $FePO_4$ sample, while part of the product was heated to 600 °C and kept sintering in air for 4 h to get amorphous precursor.

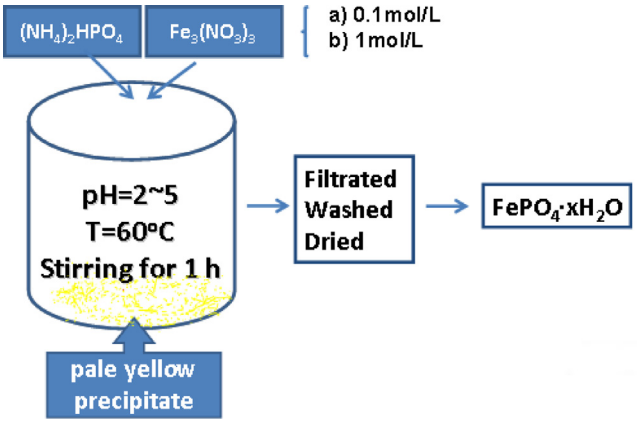

Fig. 1. Schematic illustration of preparation processes.

2.2. Synthesis of $LiFePO_4$/C composites

In order to investigate which precursor is more suitable for fabricating $LiFePO_4$, both as-synthesized $FePO_4 \cdot xH_2O$ and anhydrous $FePO_4$ after sintered at 600 °C for 4 h were used as precursors to fabricate $LiFePO_4$/C composites. Precursors were mixed with stoichiometric amount of Li_2CO_3 and an appropriate quality of glucose as carbon source for 3 h by a planetary ball mill (300 rpm). Then the mixture was dried in an oven at 80 °C for 12 h. Finally, after grinding and homogenization, the mixture was transferred to tube furnace and annealed at 720 °C for 12 h under nitrogen flow. The obtained $LiFePO_4$/C derived from as-synthesized $FePO_4 \cdot xH_2O$ was referred to as LFP-A, while the $LiFePO_4$/C prepared from anhydrous $FePO_4$ precursor as LFP-B (Table 1). In order to determine the carbon content, a certain amount of $LiFePO_4$/C composite was weighted, then dissolved it in 1:1 (vol%) HCl. After several minutes $LiFePO_4$ will be fully dissolved, in this case, the weight of the carbon in the sample can be determined.

2.3. Characterization

The phase purity and crystalline structure of as-synthesized $FePO_4 \cdot xH_2O$, anhydrous $FePO_4$ after sintered at the 720 °C temperature with the purpose to get crystalline sample, and $LiFePO_4$/C samples were characterized by XRD (DX 2700, Fangyuan DanDong) using CuKα radiation. The powder morphology and microstructures were observed by a TESCAN VEGA3-LM scanning electron microscope (SEM). The electrochemical performances of $LiFePO_4$/C composites were investigated using a CR2025 coin-type cell. The cathode electrodes were fabricated by pasting slurries of $LiFePO_4$/C (80 wt%), carbon black (10 wt%) and polyvinylidenefluride (PVDF, 10 wt%) dissolved in N-methyl-pyrrolidinone (NMP) on Al foil strips. The prepared electrode was finally dried under vacuum at 100 °C for 10 h. The electrolyte was a solution of 1 M $LiPF_6$ dissolved in the mixture solution of ethylene carbonate (EC) and dimethyl carbonate (DMC) with volume ratio of 1:1. A microporous polypropylene sheet (Celgard 2400, Celgard Inc., USA) was used as the separator. The cells were assembled in a dry glove box filled with pure argon. All the cells were allowed to age for 24 h before electrochemical evaluation. The charge–discharge tests were conducted on a battery test system (C2001A, LAND, China) with cut-off voltages of 2.5 V and 4.2 V (versus Li^+/Li) at different current rates at room temperature. The cyclic voltammetry (CV) curves were measured at 0.1 mV s^{-1} within the range of 2.5–4.2 V using Zahner IM6e Electrochemical

Table 1
Parameters of preparation $LiFePO_4$/C.

Sample	Concentration of solution (mol/L)	Processing temperature (°C)
LFP-A0.1	0.1	80
LFP-B0.1	0.1	600
LFP-A1	1	80
LFP-B1	1	600

Workstation (ZAHNER-elektrik GmbH & Co. Germany). To estimate the internal resistance of the coin-cells, the electrochemical impedance spectrum (EIS) was studied by using the same electrochemical workstation, the excitation voltage applied to the cells was 5 mV and the frequency range was between 100 kHz and 10 mHz.

3. Results and discussion

3.1. Composition, structure, morphology and other properties of $LiFePO_4$/C composites and precursors

The weight loss of 24.3% (1 M) corresponds to 2.68 molecules water per formula unit, while the weight loss for $FePO_4 \cdot xH_2O$ (0.1 M) was 23.7%, corresponding to 2.63 molecules water per formula unit. This suggests the general formula is almost $FePO_4 \cdot 2H_2O$. And the weight of the carbon in the sample was about 6 wt%.

In order to further evaluate the property of the samples, tap density measurement was carried out. Tap density of various samples is shown in Table 2. Obviously, the tap density of anhydrous $FePO_4$ was much higher than $FePO_4 \cdot xH_2O$, but it did not influence the tap density of $LiFePO_4$/C, in which the data of LEP-A0.1 was 1.20 g cm^{-3}, while LEP-B0.1 and LEP-A1 was 0.90 g cm^{-3} and 0.91 g cm^{-3}, LEP-B1 was 0.81 g cm^{-3}.

As-synthesized iron phosphate samples (both 1 M and 0.1 M) after sintering at 720 °C for 2 h were characterized by XRD. The XRD patterns (Fig. 2) demonstrate that all the diffraction peaks of the $FePO_4$ match well with the pure $FePO_4$ rodolicoite phase (PDF Card no. 04-010-9184). And the XRD patterns of four series of $LiFePO_4$/C composite are shown in Fig. 3. As seen, the olivine $LiFePO_4$ (PDF Card no. 97-015-4117) with orthorhombic *Pnma* space group is the only crystalline phase in the samples, and there do not have any big difference between the four series, except for the crystallinity of sample LFP-A1 and LFP-B0.1 was little higher than others.

The morphologies of the samples were examined with scanning electron microscopy (SEM). Fig. 4a shows the SEM image of LFP-A0.1, while Fig. 4b is for the sample LFP-A1. In Fig. 4a, the particle sizes were found to be in the range of 0.2–25 μm approximately with a size distribution quite poor. Then in Fig. 4b, the SEM photograph of LFP-A1 reveals a roughly average particle dimension of 1 μm. Importantly, it is easy to notice that LFP-A1 led to a progressive appearance with a uniform distribution. Obviously, the difference between two samples came from the unlike concentration of solution. At last, the general spherical morphology can be observed in both samples.

Table 2
Tap density of LiFePO4/C samples and precursors.

Sample	Tap density (g cm^{-3})	Tap density of precursor (g cm^{-3})
LFP-A0.1	1.20	0.37
LFP-B0.1	0.90	0.60
LFP-A1	0.91	0.48
LFP-B1	0.81	0.76

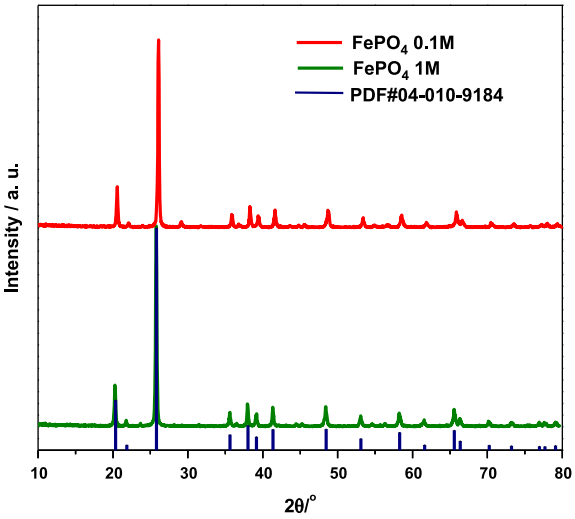

Fig. 2. XRD patterns of $FePO_4$ under different conditions.

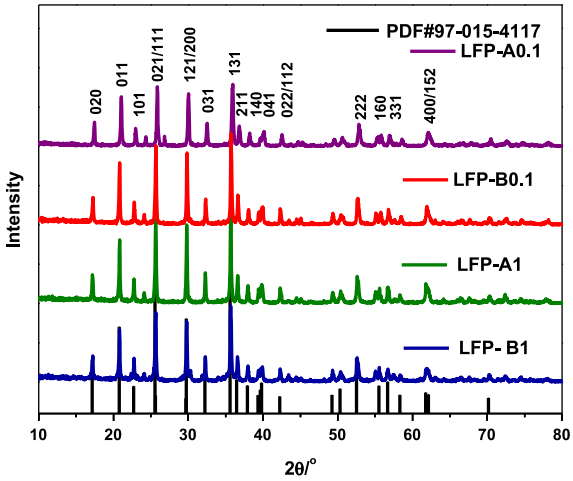

Fig. 3. XRD patterns of $LiFePO_4$/C composites synthesized from different precursors.

3.2. Electrochemical performances of $LiFePO_4$/C composites

The electrochemical performances of $LiFePO_4$/C composites were investigated by cyclic voltammetry (CV), electrochemical impedance spectroscopy (EIS) and electrochemical capacity measurement.

Fig. 5 shows the curves of cyclic voltammetry of four series after 20 charge/discharge cycles. All of the curves were speculate and well-shaped. By comparing the deviation of anodic peak and cathodic peak with each other, it is clearly that LFP-A1 shows the best reversibility and minimum polarization with the deviation 0.336 V at scanning rate of 0.5 mV s^{-1} (0.226 V at 0.1 mV s^{-1}).

Then, EIS experiments were carried out at equilibrium state on coin cells after 20 cycles (Fig. 6a). The impedance behavior included one semicircle followed by linear part. On the basis

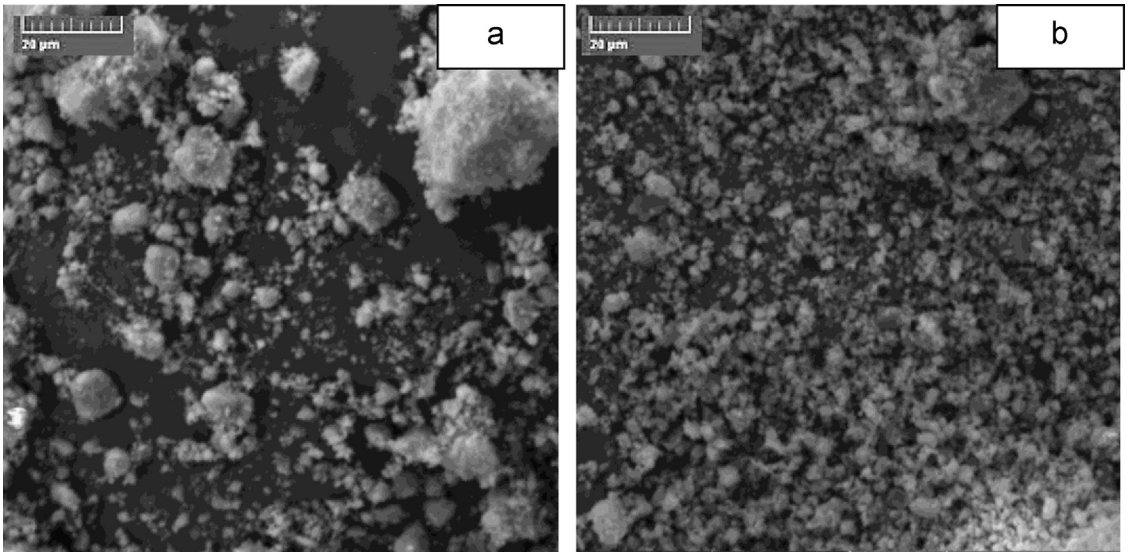

Fig. 4. a: SEM image of LFP-A0.1 sample. b: SEM image of LFP-A1 sample.

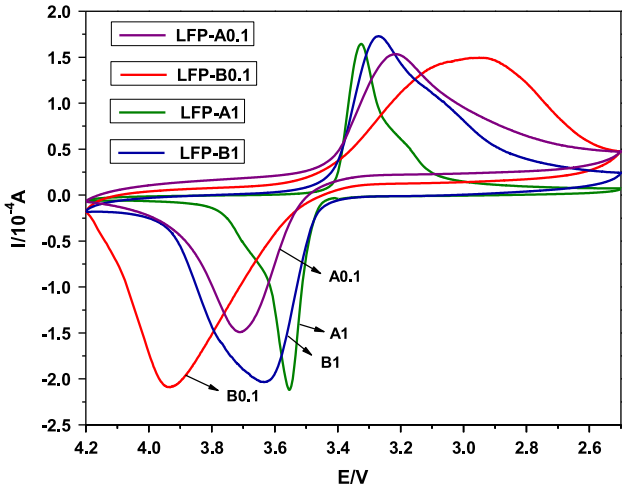

Fig. 5. Cyclic voltammogram of four series, scanning rate: 0.5 mV s^{-1}, voltage range: 2.5–4.2 V.

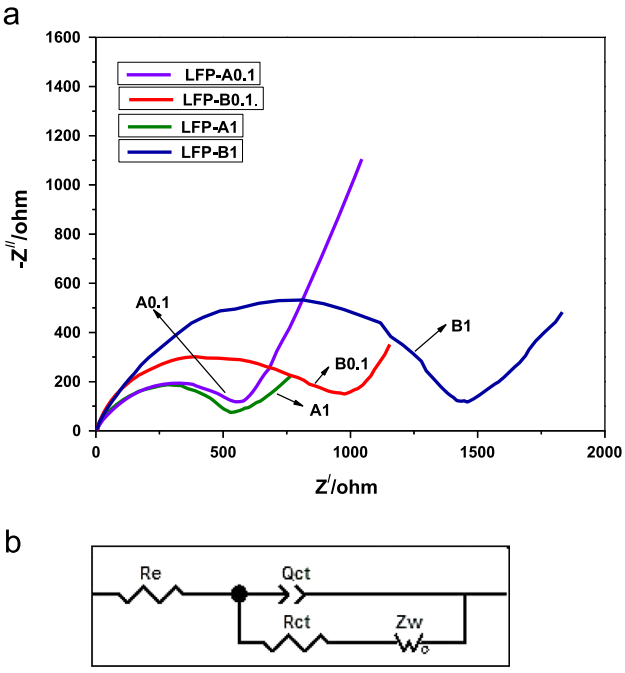

Fig. 6. a: EIS of four series, frequency: 10^5–0.1 Hz for LEP-A1, LEP-A0.1, LEP-B0.1, 10^5–0.01 Hz for LEP-B1; b: the equivalent circuit diagram of impedance spectra.

of curve shape, the equivalent circuit model of impedance spectra was set to include an electrolyte resistance (R_e), a charge transfer resistance (R_{ct}) after that, and a series circuit consist of a double layer and passivation film capacitance (Q_{ct}) and a warburg impedance (Z_w) in parallel with R_{ct} (as Fig. 6b). Again, LFP-A1 has the smallest semidiameter, presents that electrochemical polarization of LFP-A1 is the smallest one in these four series. By the means of fitting and simulation, the numerical values of R_e, R_{ct}, Q_{ct} and Z_w for four series were obtained, part of these values are listed in Table 3. It is clear to see that the R_{ct} of LFP-A1 was lower than others, simultaneously, the i^0 of LFP-A1 was the largest one, which means LFP-A1 got the best electrochemical performance.

Table 3
Part of values obtained from fitting of EIS.

Sample	R_e (Ω)	R_{ct} (Ω)	i^0 (10^{-4} A)
LFP-A0.1	3.6	577	4.37
LFP-B0.1	3.3	841	3.00
LFP-A1	5.2	509	4.96
LFP-B1	3.6	1392	1.81

Electrochemical capacity measurement was carried out in the potential range of 4.2–2.5 V at different rates from 4*C* to 0.1*C*. In Fig. 7, the initial charge/discharge curves of the four series at 2*C* were shown. The first charge capacity of LFP-A1, LFP-B0.1, LFP-A0.1, LFP-B1 is about 101 mAh g^{-1}, 82 mAh g^{-1}, 69 mAh g^{-1}, 58 mAh g^{-1}, and the first discharge capacity is 97 mAh g^{-1}, 70 mAh g^{-1}, 52 mAh g^{-1}, 44 mAh g^{-1} in

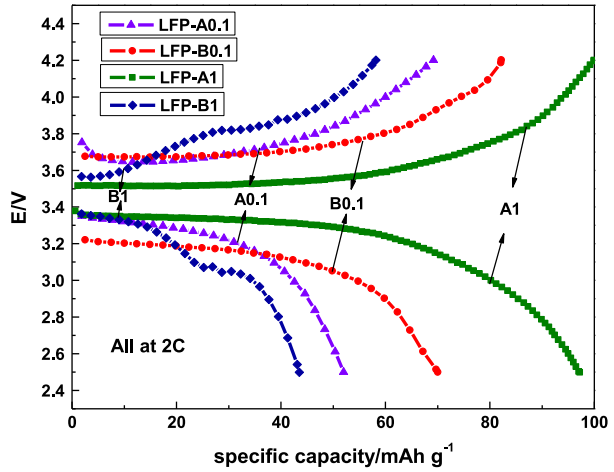

Fig. 7. Initial charge/discharge curves of the four series at 2*C*.

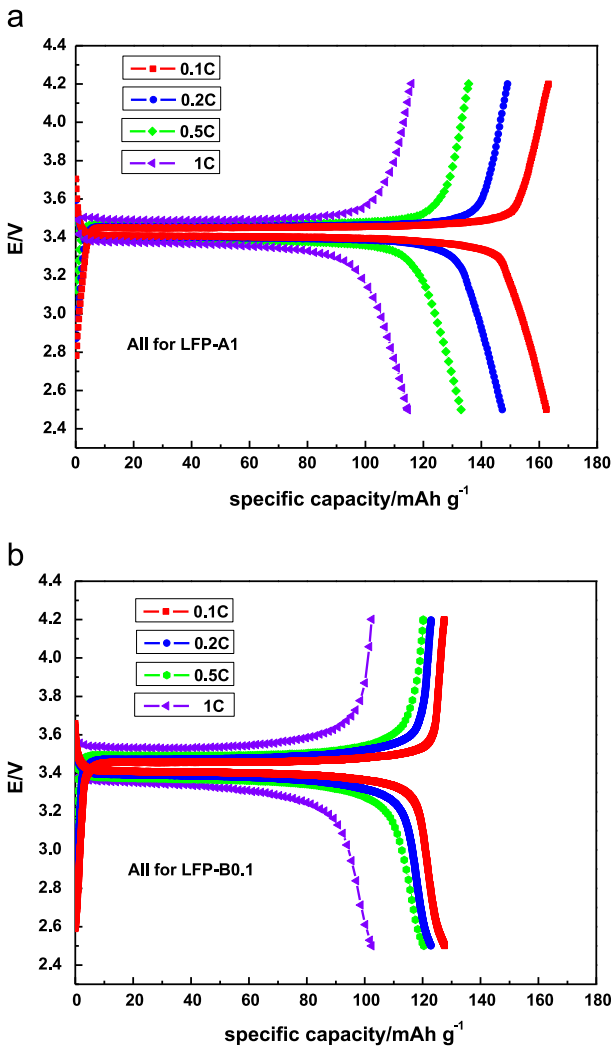

Fig. 8. a: Charge/discharge curves of LFP-A1 sample at rates of *C*, 0.5*C*, 0.2*C* and 0.1*C*. b: Charge/discharge curves of LFP-B0.1 sample at rates of *C*, 0.5*C*, 0.2*C* and 0.1*C*.

descending order at a relatively high rate of 2*C*. It was clear that LFP-A1 exhibits the best electrochemical performance, and LFP-B0.1 ranks only second to LFP-A1.

The charge/discharge curves of LFP-A1 at rates of 1*C*, 0.5*C*, 0.2*C* and 0.1*C* were shown in Fig. 8a. It can deliver the discharge capacity of 114.7 mAh g^{-1}, 133.0 mAh g^{-1}, 147.3 mAh g^{-1}, 162.5 mAh g^{-1} at rates of 1*C*, 0.5*C*, 0.2*C* and 0.1*C*, respectively. The cycle of LFP-A1 at the rate of 0.1*C* is shown with the charge capacity of 163.0 mAh g^{-1} and the discharge capacity of 162.3 mAh g^{-1}, which is very close to the theoretical capacity. And the lithium is extracted from $LiFePO_4$ along a flat potential at 3.44 V versus Li and inserted into $FePO_4$ along a flat potential at 3.41 V versus Li. During the discharge step, the cathode was able to accommodate about 90% of the total capacity before the voltage drops below 3.30 V and then fell sharply. Then, the charge/discharge curves of LFP-B.1 at rates of 1*C*, 0.5*C*, 0.2*C* and 0.1*C* were shown in Fig. 8b. It can deliver the discharge capacity of 102.3 mAh g^{-1}, 120.0 mAh g^{-1}, 123.0 mAh g^{-1} and 127.0 mAh g^{-1} at rates of 1*C*, 0.5*C*, 0.2*C* and 0.1*C*, respectively. Compared with LFP-A1, LFP-B0.1 always had a lower capacity at the same rate.

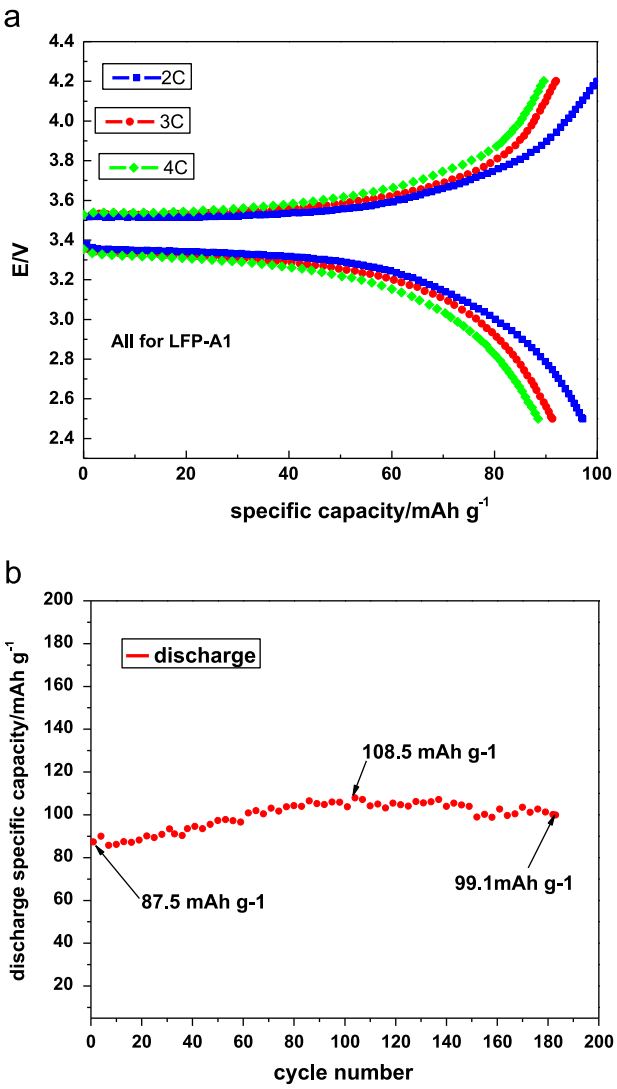

Fig. 9. a: Charge/discharge curves of LFP-A1 sample at rates of 4*C*, 3*C* and 2*C*. b: Charge/discharge capacity upon cycling of LFP-A1 sample.

To study further, the charge/discharge curves of LFP-A1 at rates of 4*C*, 3*C* and 2*C* were shown in Fig. 9a. It can deliver the discharge capacity of 88.5 mAh g^{-1}, 91.3 mAh g^{-1} and 97.2 mAh g^{-1} at rates of 4*C*, 3*C* and 2*C*, respectively. Then, the cycle performance of LFP-A1 was presented in Fig. 9b. It delivered an initial discharge capacity of 87.5 mAh g^{-1} and a capacity of 91.6 mAh g^{-1} at the 3th cycle. And the discharge capacity kept on rising to 108.5 mAh g^{-1} at 105th cycle, then kept on decaying to 99.1 mAh g^{-1} at 180th cycle. The improved capacity can be related to the slow penetration of electrolyte through the microstructure in the $LiFePO_4$/C particles [20] and the generation and enlargement of crack as the cycle number increasing.

4. Conclusions

In this paper, the co-precipitation method has been used to prepare $FePO_4 \cdot xH_2O$ to fabricate cathode material $LiFePO_4$/C composites. In summary, the $LiFePO_4$/C sample LFP-A1 synthesized from $FePO_4 \cdot xH_2O$ which was obtained from solution of 1 mol/L and only dried at 80 °C, has the best electrochemical performance. It can deliver discharge capacities of 162.5 mAh g^{-1}, 147.3 mAh g^{-1}, 133.0 mAh g^{-1}, 114.7 mAh g^{-1}, 97.2 mAh g^{-1}, 91.3 mAh g^{-1} and 88.5 mAh g^{-1} at rates of 0.1*C*, 0.2*C*, 0.5*C*, 1*C*, 2*C*, 3*C* and 4*C*, respectively, with satisfactory capacity retention.

References

[1] B.Q. Zhu, X.H. Li, Z.X. Wang, et al., Novel synthesis of $LiFePO_4$ by aqueous precipitation and carbothermal reduction, Mater. Chem. Phys. 98 (2006) 373–376.
[2] L.F. Jiao, W.X. Peng, H.Y. Gao, et al., Enhanced electrochemical performance of $LiFePO_4$/C via Mo-doping at Fe site, Electrochim. Acta 56 (27) (2011) 9961–9967.
[3] X.F. Zhou, F. Wang, Y.M. Zhu, et al., Graphene modified $LiFePO_4$ cathode materials for high power lithium ion batteries, J. Mater. Chem. 21 (2011) 3353–3358.
[4] A.K. Padhi, K.S. Nanjundaswamy, J.B. Goodenough, Phospho-olivines as positive-electrode materials for rechargable lithium batteries, J. Electrochem. Soc. 144 (1997) 1188–1190.
[5] Z.C. Shi, A. Attia, W.L. Ye, et al., Synthesis, charactherization and electrochemical performance of mesoporous $FePO_4$ as cathode materials for rechargeable lithium batteries, Electrochim. Acta 53 (2008) 2665–2673.
[6] T.F. Yi, X.Y. Li, H.P. Liu, et al., Recent developments in the doping and surface modification of $LiFePO_4$ as cathode material for power lithium ion battery, Ionics 18 (2012) 529–539.
[7] W.X. Peng, L.F. Jiao, H.Y. Gao, et al., A novel sol–gel method based on $FePO_4 \cdot 2H_2O$ to synthesize submicrometer structured $LiFePO_4$/C cathode material, J. Power Sources 196 (5) (2011) 2841–2847.
[8] D.P. Jiang, X.J. Zhang, S.G. Lu, et al., Research on process of preparation and performance of iron phosphate as precusor of lithium iron phosphate, Rare Met. 30 (2011) 52–54.
[9] L. Jing, G.L. Yang, X.F. Zhang, et al., Synthesis of the $LiFePO_4$/C core–shell nanocomposite using a nano-$FePO_4$/polythiophene as an iron source, J. Power Sources 197 (2012) 253–259.
[10] L.N. Wang, Z.G. Zhang, K.L. Zhang, A simple, cheap soft synthesis routine for $LiFePO_4$ using iron (III) raw material, J. Power Sources 167 (2007) 200–205.
[11] S. Okada, T. Yamamoto, Y. Okazaki, et al., Cathode properties of amorphous and crystalline $FePO_4$, J. Power Sources 146 (2005) 570–574.
[12] L.C. Qian, Y. Xia, W.K. Zhang, et al., Electrochemical synthesis of mesoporous $FePO_4$ nanoparticles for fabricating high performance $LiFePO_4$/C cathode materials, Microporous Mesoporous Mater. 152 (2012) 128–133.
[13] S.M. Zhu, H.S. Zhou, M. Hibino, et al., Synthesis of hexagonal mesostructured $FePO_4$ using cationic surfactant as the template, Chem. Lett. 33 (6) (2004) 774–775.
[14] M. Wang, Y.H. Xue, K.L. Zhang, et al., Synthesis of $FePO_4 \cdot 2H_2O$ nanoplates and their usage for fabricating superior high-rate performance $LiFePO_4$, Electrochim. Acta 56 (2011) 4294–4298.
[15] X.F. Guo, W.P. Ding, X.G. Wang, et al., Synthesis of a novel mesoporous iron phosphate, Chem. Commun. 8 (2001) 709–710.
[16] W.J. Zhou, W. He, X.D. Zhang, et al., Biosynthesis of iron phosphate nanopowders, Powder Technol. 194 (2009) 106–108.
[17] F. Cao, D.X. Li, Biotemplate synthesis of monodispersed iron phosphate hollow microspheres, Bioinspir. Biomim. 5 (2010) 1748–3182.
[18] S. Scaccia, M. Carewska, P.P. Prosini, Thermoanalytical study of iron (III) phosphate obtained by homogeneous precipitation from different media, Thermochim. Acta 413 (1–2) (2004) 81–86.
[19] K. Mal, A. Bhaumik, M. Matsukata, et al., Syntheses of mesoporous hybrid iron oxophenyl phosphate, iron oxophosphate, and sulfonated oxophenyl phosphate, Ind. Eng. Chem. Res. 45 (2006) 7748–7751.
[20] J.F. Ni, H.H. Zhou, J.T. Chen, et al., Molten salt synthesis and electrochemical properties of spherical $LiFePO_4$ particles, Mater. Lett. 61 (2007) 1260–1264.